Injectable Gelatin Microgel-based Composite Ink for 3D Bioprinting in Air

Kaidong Song[1, $], Ashley M. Compaan[2, $, #], Wenxuan Chai[1], Yong Huang[1, 2, *]

[$] Equal contribution

[1]Department of Mechanical and Aerospace Engineering, University of Florida, Gainesville, FL 32611, USA.

[2]Department of Materials Science and Engineering, University of Florida, Gainesville, FL 32611, USA.

[$] Equal contribution

[#]Novabone Products, LLC. 13510 NW US Highway 441, Alachua, FL, 32615 USA.

[*]Corresponding author

Keywords: injectable, hydrogel composite, printing in air, bioprinting, cross-linkable composite ink

Abstract

Injectable hydrogels have attracted much attention in tissue engineering and regenerative medicine for their capability to replace implantation surgeries with a minimally invasive injection procedure and ability to fill irregular defects. The proposed composite ink is a gelatin microgel-based yield-stress and shear-thinning composite material that is injectable and solidifies quickly after injection at room temperature, which can be utilized for creation of three-dimensional (3D) parts in air directly. The gelatin composite ink consists of a microgel solid phase (gelled gelatin microgels)

and a cross-linkable solution phase (gelatin solution-based acellular or cellular suspension). The gelatin composite ink can be injected or printed directly in air and solidifies as physical cross-linking to hold printed structures at room temperature. The fabricated part further undergoes chemical cross-linking process by being immersed in a transglutaminase (TG) solution to enzymatically gel the gelatin solution, making a physiologically stable construct as needed. Lattice, tube-shaped, cup-shaped, and human anatomical (ear and nose) structures are printed to demonstrate the feasibility of the proposed composite ink for printing applications. The morphology and metabolic activity of cells cultured in the gelatin composite ink are further analyzed to confirm the suitability of the proposed composite ink to provide a beneficial physiological environment for bioprinting needs.

1. Introduction

Tissue engineering and regenerative medicine are interdisciplinary research areas which combine the principles of materials engineering and life sciences with the development of technologies that can restore, maintain and improve tissue functions [1]. While the transplantation of tissue or organ is a generally accepted therapy to treat patients with diseased or failed tissues/organs, this approach is still limited by the challenge of organ donor shortage. Fortunately, the field of tissue engineering and regenerative medicine has been developed to meet the tremendous need for organs and tissues [2]. The enabling component of most tissue engineering and regenerative medicine strategies is the customized creation of engineered tissues or cell-laden scaffolds, which can be implanted into a patient. Ideal cell-laden scaffolds should be made from living cells and extracellular matrix (ECM) materials, the ECM material is often in the form of a hydrogel to provide structural and biochemical support for surrounding cells. Hydrogels are three-dimensional (3D) cross-linked

water-saturated polymer networks, providing an appropriate microenvironment similar to the ECM of healthy tissues [3-6].

Among different hydrogels used for scaffolds, injectable hydrogels have attracted much attention in tissue engineering and regenerative medicine for their capability to replace implantation surgeries with a minimally invasive injection procedure and ability to fill irregular defects [7-11]. The ability for a hydrogel to be injected homogenously via a cannulated needle, a property called injectability [12], is one of the most important properties when considering its application in minimally invasive surgery as well as biological construct fabrication. Injectable hydrogels can be prepared using either physical or chemical methods. Physical injectable hydrogels are produced by weak secondary forces spontaneously while chemical hydrogels are usually produced by covalent cross-linking [13-15]. Generally, injectable hydrogels can be prepared from a variety of biomaterials, both natural and synthetic, including chitosan [8], collagen or gelatin [16,17], alginate [18], hyaluronic acid [19], heparin [20], chondroitin sulfate [21], poly (ethylene glycol) (PEG) [22], Fmoc-tyrosine-aspartic acid/Fmoc-tyrosine-lysine [23] and poly (vinyl alcohol) (PVA) [24]. While typical injectable hydrogels are often shear thinning, which allows for good injectability after subjecting them to stress, it is also desirable for them to gel right after injection in order to have prompt recovery of mechanical properties *in situ* and retain their shape as deposited. The latter property enables the use of such injectable hydrogels for numerous applications, such as bioinks in 3D bioprinting applications, especially extrusion-based 3D bioprinting [25,26]. For extrusion-based 3D bioprinting applications, injectable hydrogel-based shear-thinning bioink passes through a nozzle and gels *in situ* to form functional 3D structures with satisfactory cell viability for further maturation and implantation.

Despite the promising results of developed injectable hydrogels for 3D bioprinting applications that have been reported, most of them are still not ideal for robust bioprinting. Alginate has the main drawbacks of nondegradability and lack of intrinsic cell-adhesive motifs [27]. Chitosan is a soft biomaterial under hydrated conditions and its low mechanical stiffness limits its use without the addition of other components [28]. PVA is not biodegradable in most physiological situations [29] and insufficient in mechanical stability [30]. Gelatin, a water-soluble protein derived from collagen [29], is a desirable material for its good thermal stability with enzymatic cross-linking and biodegradability. However, its utilization at a working temperature (T) near its sol-gel transition point (upper critical transition temperature (UCST) or $T_{sol\text{-}gel}$ which is around 25-35 ºC [31]) is complicated by the abrupt transition from hydrogel ($T < T_{sol\text{-}gel}$) to a low-viscosity fluid ($T > T_{sol\text{-}gel}$). As a result, gelatin either does not flow well or flows uncontrollably during fabrication depending on the printing temperature, resulting in poor print fidelity. Considering the wide tissue engineering applications and low cost of gelatin and its derivatives [32,33], there is a need for an improved gelatin or gelatin-based biomaterial for robust 3D bioprinting while avoiding possible ultraviolet-induced cell damage and impaired tissue formation associated with methacrylated gelatin [34,35].

This study aims to develop an injectable gelatin-based composite ink for use in 3D bioprinting, which consists of a gelatin continuous phase and gelatin microgels. The use of gelatin in both phases ensures complete biocompatibility and susceptibility to cell-mediated degradation and remodeling. By forming a composite consisting of both covalently cross-linked gelatin microgels and native gelatin, the rheological properties can be controlled without non-gelatin additives,

which is mainly achieved by adding gelatin microgels prepared under different gelatin concentrations. Microgels, which are hydrogels in the form of micron-scale particles, are valuable as rheology modifiers. Microgels in a jammed composite system are densely packed and restricted with surrounding microgels by physical interactions, resulting in a macroscopic material that behaves as solid until enough force is applied to induce movement [36-40]. Nearly any hydrogel can be processed to produce microgels including alginate [41], hyaluronic acid (NorHA) [42], poly (ethylene glycol) diacrylate (PEGDA) [42] and agarose [42] although the properties of packed microgels vary depending on the intrinsic properties of each hydrogel material as well as the size and shape distributions of the microgels themselves. Gelatin hydrogel is chosen as the microgel material in this study since packed gelatin microgels are not only as cell-responsive as gelatin itself but also enhances the effective viscosity and yield-stress behavior of the resulting ink. As such, well-defined constructs can be fabricated using the proposed injectable hydrogel composite ink.

In this study, an application of sufficient stress to the composite consisting of a continuous gelatin solution phase and jammed gelatin microgel filler results in movement of the gelatin microgels relative to each other as stress surpasses the packing force that resists motion. Once the applied stress is below the yield stress, the gelatin composite system recovers and behaves as a solid at rest. This flow and recovery of the jammed gelatin microgel system in response to stress meet the design requirements of inks for 3D bioprinting. Because the gelatin microgels impart yield-stress behavior to the gelatin composite, the resulting composite ink can be printed in air without immediately requiring rapid irreversible solidification to form 3D structures. Furthermore, chemical cross-linking of the continuous gelatin phase solution after printing results in a covalently cross-linked continuous gelatin phase entrapping with the gelatin microgels throughout the entire

printed structure. Since chemical cross-linking happens after printing is complete, it promotes better fusion between deposited layers and mitigates interfacial weakness. Thus, the proposed injectable gelatin composite enables the printing of mechanically stable, biocompatible, biodegradable, and tunable constructs without involving complicated cross-linking process, which may be utilized as custom tissue models, in vitro test platforms, and in vivo tissue regeneration aids.

2. Design of Gelatin-gelatin Composite as Injectable Hydrogel

Gelatin is a water-soluble protein derived from collagen. Due to its good biocompatibility and biodegradability and ability to form hydrogels, gelatin is widely used in applications ranging from the food industry to medicine and tissue engineering. Gelatin can form physical hydrogels via physical interactions between helical regions of the protein. The thermoreversible hydrogel formed by aqueous gelatin has a UCST of 25-35°C [31]. When the temperature exceeds this critical point, the hydrogel liquefies as the helical region become random coils. Although the sol-gel transition of the thermoreversible gelatin can be exploited for bioprinting such that gelatin transitions from a low viscosity fluid (inside a dispensing tip) to a physically cross-linked hydrogel (outside the dispensing tip), the transition process is usually too quick to control during printing, resulting in poor print fidelity. For better printability of unmodified gelatin, its ink formulation must be adjusted accordingly.

Herein jammed gelatin-based microgels are chosen as the rheology modifier for the gelatin solution to prepare the proposed injectable yield-stress and shear-thinning gelatin microgel-based composite ink since the gelatin-based microgels have the same cell-responsive characteristics of

the continuous gelatin phase. To form gelatin-based constructs which are stable at physiological conditions, a variety of cross-linking methodologies and chemistries have been developed. One of the mildest and most convenient cross-linking reactions relies on microbial transglutaminase (TG), an enzyme that is highly active at physiological conditions and catalyzes the formation of covalent bonds between protein molecules. As such, TG is used as a physiological cross-linking agent to produce thermostable gelatin structures so that the printed structures are suitable for tissue engineering and regenerative medicine applications including implantation. While TG has been used for different gelatin bioprinting applications [43], During and after printing, each printed structure herein is solidified rapidly first by physical cross-linking of the gelatin microgels related to the microgel unjamming-jamming transition (strictly speaking, partially due to the thermal gelation of the gelatin solution too) and then by slow enzymatic cross-linking of the gelatin solution by TG. Such a TG-based mild cross-linking approach also avoids possible cross-linking damage (such as ultraviolet damage) when using chemically modified gelatins for printing and cross-linking.

The printing process using the injectable gelatin microgel-based composite ink is illustrated in **Figure 1**. Before printing, gelatin microgels in the composite ink are restricted as jammed as shown in **Figure 1a-1** through physical interactions with surrounding microgels, resulting in solid-like behavior. When the ink passes through the extrusion nozzle tip, it is subjected to sufficient shear stress, which liquefies the composite ink (**Figure 1a-2**) and enables smoothly flowing deposition in controlled spatial patterns. After deposition, the unjammed liquid-like microgels within the composite mixture recover to solid-like behavior and retain the printed configuration due to the jamming and cooling effect (**Figure 1a-3**). For gelatin-based composite ink stabilization,

the continuous gelatin solution phase may include TG as a cross-linking agent during the ink preparation phase if the printing time is short enough, typically 45 minutes, for the composite ink to maintain its yield-stress property during the TG-initiated cross-linking process. **Figure 1a-4** and **1a-5** shows the continuous gelatin phase of the composite ink without or with TG, respectively, during printing, and **Figure 1a-6** and **1a-7** shows the continuous gelatin phase of the composite ink without or with TG, respectively, after printing.

During the post-printing stage (**Figure 1b**), if the continuous gelatin phase does not include TG, the printed structure is immersed in a TG solution for the chemical cross-linking of the continuous phase (**Figure 1b-1**); if the continuous gelatin phase includes TG, the printed structure is directly incubated at 37°C for further chemical cross-linking (**Figure 1b-2**).

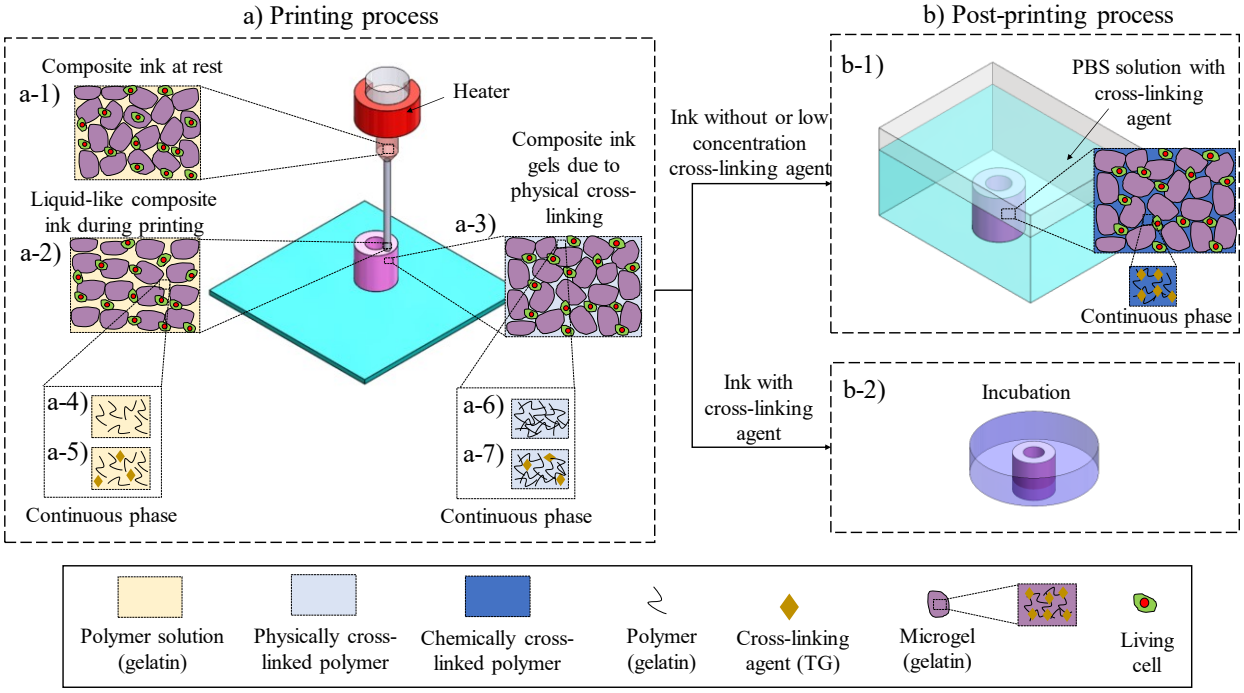

Figure 1. Schematics of direct printing of gelatin microgel-based composite ink. (a) Composite ink direct printing in air: (a-1) Composite ink stored in a dispensing syringe. Composite ink (a-2) passes through a nozzle and undergoes shear-thinning and (a-3) solidifies immediately after deposition due to physical cross-linking upon jamming and cooling. Composite ink (for example, gelatin-based herein) (a-4) without and (a-5) with a cross-linking agent (for example, TG herein). Physically cross-linked polymer (gelatin) (a-6) without and (a-7) with the cross-linking agent (TG). (b) Post-printing process: (b-1) cross-linking in a cross-linking agent bath for structures printed from inks without or low concentration cross-linking agent and (b-2) cross-linking in an incubation environment for structures printed from inks with cross-linking agent.

3. Composite Ink Characterization and Discussion

3.1 Self-supporting property assessment of gelatin microgel-based composite ink

The rheological properties of the gelatin microgel-based composite ink (3% gelatin with 10% gelatin microgels, and no TG) were measured to elucidate the sol-gel transition behavior and the self-supporting property of the ink during the printing process. The yield-stress property is investigated by sweeping the shear stress and recording the shear moduli and presented in **Figure 2a** and **S1a** of the **supporting information SI1**. As seen from **Figure 2a**, when the shear stress is relatively low, the storage modulus of gelatin microgel-based composite ink is higher than its loss modulus, which indicates that the composite ink remains jammed and presents solid-like behavior. When the shear stress of the composite ink is higher than a critical value to induce an unjammed state, the storage modulus becomes lower than the loss modulus, resulting in fluid-like behavior of the composite ink. As such, the composite ink can be easily injected through a cannulated

needle, and this critical shear stress value is the yield stress of suspension. The shear-thinning behavior of the gelatin microgel-based composite ink is shown in **Figure 2b** and **S1b**. It is found that the viscosity of gelatin microgel suspensions decreases with the shear rate. Under stressed conditions, the microgels distribute along the stress direction and become unjammed, resulting in the decrease of viscosity. Therefore, the ink can pass through the extrusion tip easily as a result of its shear-thinning behavior. It is noted that temperature is an important factor for yield stress (the intersection point of shear moduli) and viscosity as shown in **Figure 2a** and **2b**: a higher temperature results in a lower yield stress and lower viscosity. The shear-thinning through low and high strain cycles under different concentrations and temperatures are studied and shown in **Figure S1c** and **S1d**, respectively.

All the suspensions at different gelatin concentrations can reversibly switch the states between fluid- and solid-like in a relatively short time. **Figure 2c** shows the relationship between the viscosity and the time under transient zero-shear rate measurements. The viscosity of the composite ink in the shear zone is low (around 4.6 Pa • s) due to the shear-thinning effect, while the viscosity increases rapidly to around 80 Pa • s after the shear rate decreases to 0 s^{-1} in approximately 0.2 s. This short response time indicates that the ink dispensed can quickly return to solid-like behavior after being liquefied by the dispensing process, thus retaining the deposited shape and forming well-defined constructs.

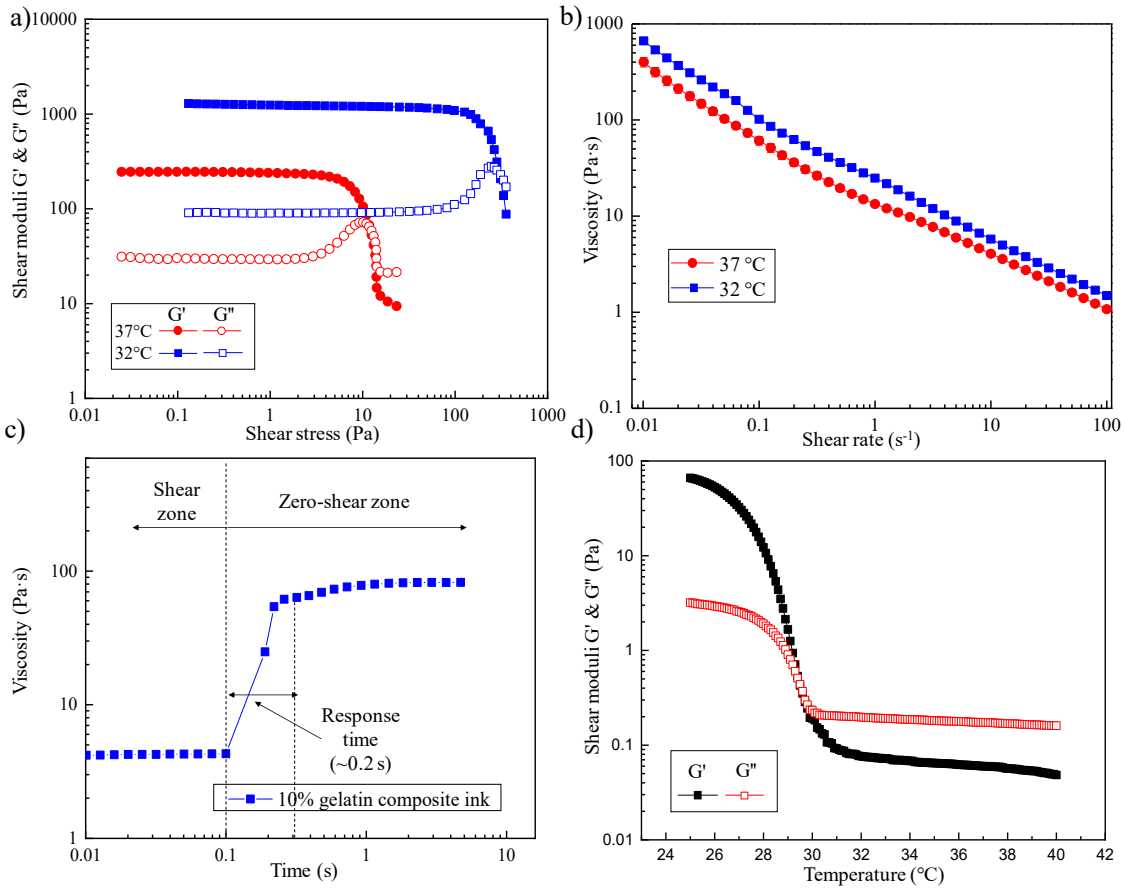

Figure 2. Rheological property measurements. (a) Yield stress at different temperatures. (b) Apparent viscosity at different temperatures under steady shear. (c) Viscosity jump after a response time during transient zero-shear rate measurements. (d) Shear modulus at an angular frequency of 1 Hz and an oscillatory strain of 1% during cooling from 40°C to 25°C to show the critical transition point.

To print a thermoresponsive hydrogel, it is of importance to identify the temperature for sol-gel transition and further accurately control the temperature for printing applications at a liquid-like state. Herein a temperature sweep was performed on a 3% gelatin solution to find the critical sol-gel transition point of the continuous gelatin solution phase. As shown in **Figure 2d**, the 3% gelatin

solution exhibits fluid-like behavior at high temperatures, where the loss modulus is higher than the storage modulus. As the temperature drops below a critical point (approximately 30 °C), the storage modulus exceeds the loss modulus because of the formation of a physical gelatin network. It undergoes rapid gelation, which allows the composite ink to form a gel structure. Square patterns (**Figure S2a-2c**) were printed on paper substrates at low (below 30 °C), middle (around 32 °C), and high (above 37°C) temperatures to show the influence of temperature on the printing process. As observed, 30°C is selected as the working temperature for good printability.

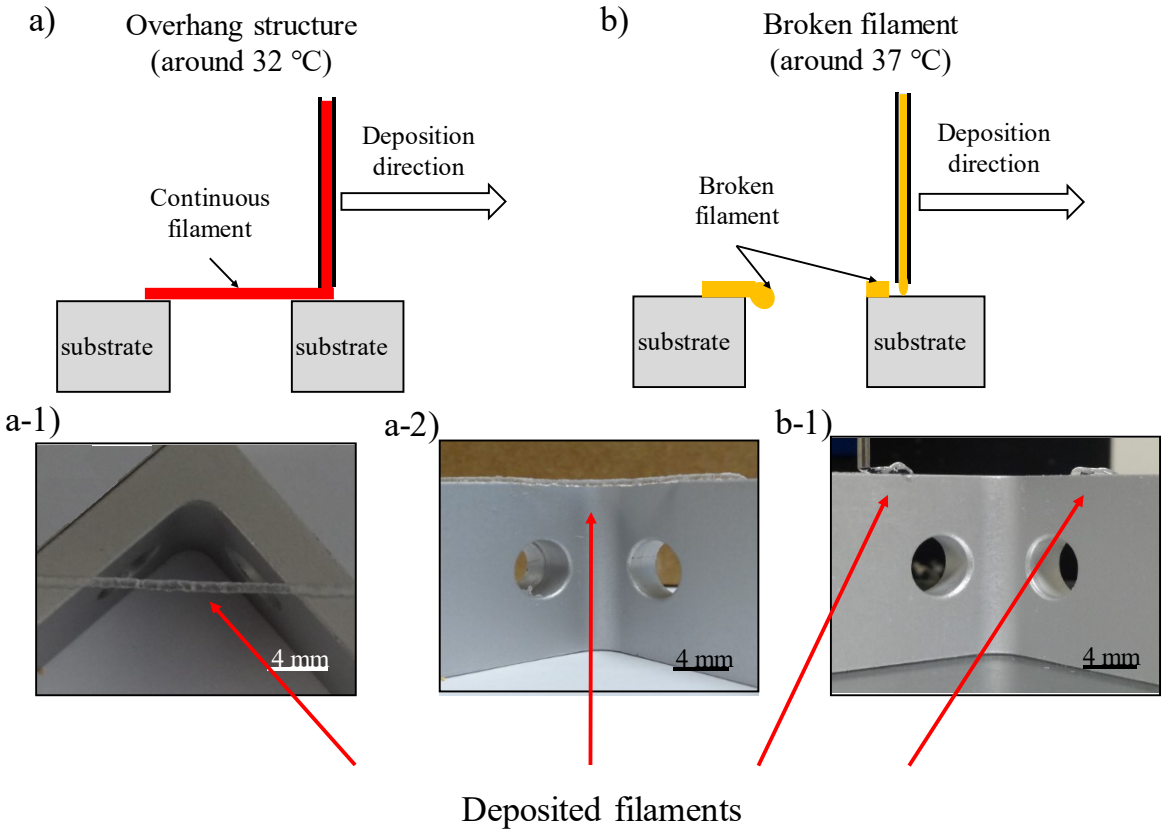

Figure 3. Characterization of temperature effects on composite ink's self-supporting property. (a) Schematic of continuous filament deposition. (a-1) Top view and (a-2) front view of a spanning filament. (b) Schematic of deposition with broken filaments and (b-1) front view of a broken filament.

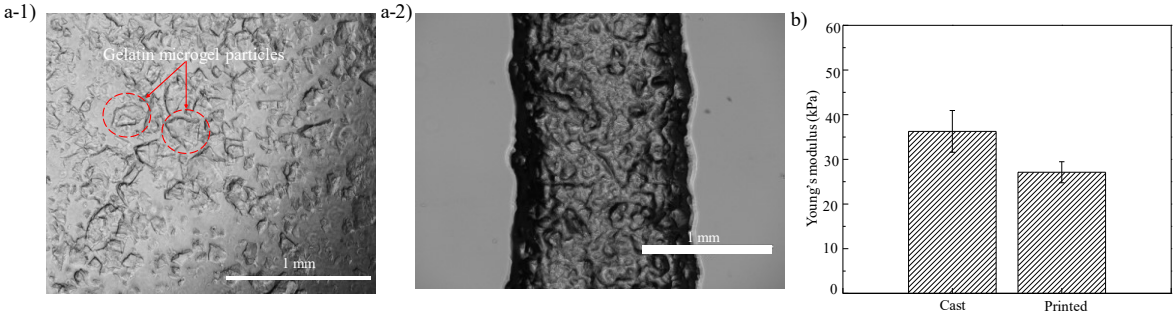

Figure 4. (a-1) Gelatin microgel particle (10% gelatin 5 min blending) (Reprinted (adapted) with the permission from ACS Applied Materials. Copyright 2020 American Chemical Society) and (a-2) gelatin microgel composite ink after printing (3% gelatin with 10% gelatin microgels). (b) Young's modulus of gelatin microgel-based composites as cast and printed (10% gelatin microgels)

Furthermore, spanning filaments were printed to evaluate the self-supporting capability of the designed gelatin-based composite ink (3% gelatin with 10% gelatin microgels) as shown in **Figure 3a** and **3b**. As shown in **Figure 3a**, the gelatin microgel-based composite ink can form filaments with well-defined geometry on a supporting structure. When extruding beyond the supporting structure, the extruded composite ink switches its state from liquid-like to solid-like rapidly due to physical cross-linking, which results in a relatively rigid filament that holds its shape in air. In contrast, a filament extruded at a higher temperature (such as 37 °C) doesn't have a sol-gel

transition to be solid-like after dispensing based on the shear moduli information shown in **Figure 2d** and cannot support a spanning structure effectively as illustrated in **Figure 3b**. The self-supporting capacity of the gelatin composite ink can be predicted by calculating the maximum shear stress and maximum tensile stress (**supporting information SI2**).

It should be pointed out that the gelatin microgels can also improve the print fidelity as shown in **Figure S2b** and **S2d**. For the ink without microgels, the corners of the printed spiral pattern are not as sharp as those inks with microgels. The printed line morphology is strongly dependent on the gelatin microgel size. The finer the gelatin microgel, the better the line morphology. The average size of gelatin microgels can be controlled by varying either the gelatin concentration or blend time as seen from **Figure S3**, respectively, and 5 min has been chosen as the blend time for material preparation since a longer blend time has little impact on the microgel size. **Figure 4a-1** shows the morphology of some gelatin microgel beads (10% gelatin 5 min blending) and **Figure 4a-2** shows the morphology of deposited gelatin microgel-based composite ink (3% gelatin with 10% gelatin microgels) under an optical microscope.

The typical printing temperature is controlled at 32 °C; the gelatin solution continuous phase experiences rapid physical cross-linking due to the temperature drop (to the room temperature) after printing. To ensure the mechanical stiffness of printed structures, TG is added into the gelatin microgel-based composite ink to have further chemical cross-linking of the gelatin solution in addition to its physical cross-linking. The mechanical properties of the chemically cross-linked gelatin microgel-based composites were investigated using tensile testing (**supporting information SI3**). It can be seen that the stress of the cross-linked gelatin microgel composites

(3% gelatin with 5%, 10%, and 15% gelatin microgels) increases linearly with the strain in the elastic region. Under an additional strain, the composites undergo plastic deformation, and the stress increases significantly.

The effective Young's modulus [44] of the cast composites at different concentrations is determined to be around 14.4 kPa, 36.3 kPa, and 56.8 kPa, respectively based on the slopes of the linear region of the stress-strain curves. The average Young's modulus of the printed 10% gelatin microgel-based composites is a little lower (27.1 kPa) than that of the cast parts (36.3 kPa) but on the same order of magnitude, which demonstrates the good mechanical properties of the structures printed using the designed gelatin composite ink (**Figure 4b**). The average Young's modulus of the printed parts is in the same range (0.1 kPa to 10 kPa) [45] of many native tissues: such as liver, brain, and adipose. If needed, the mechanical strength can be enhanced using some additives such as biocompatible nanoclay particles. It is noted that all structures were printed using a 10% gelatin microgel-based composite ink (with a 3% gelatin continuous phase) since the 5% gelatin microgel-based composite ink is too weak to hold the structure, and a higher polymer concentration is not favorable for cell proliferation [45].

The Young's modulus of the designed gelatin microgel-based composite (27.1 kPa for 10% gelatin microgels) is lower when compared with other gelatin-based materials for tissue engineering such as gelatin-methacryloyl (GelMA) (43.0 kPa for 10%) [46], gellan gum methacrylate (GGMA) and GelMA double-network hydrogel (80.0 kPa for 0.5% GGMA hydrogels and 20% GelMA) [47] and gelatin methacryloyl with chitin nanofibers (GMAC) (2.8 to 4.6 MPa) [48]. The low Young's modulus makes composite structures more flexible and easier to handle for tissue engineering

applications and more closely match the mechanical properties of healthy tissues. **Figure S3** also illustrates the ductility of the designed composites, showing that the dog bone-shaped specimen could be elongated up to 20 mm (approximately 350%) without any breakage (**Movie M1**).

3.2 Injectability and printability study

Injectability, the capability for hydrogel-based materials to be homogenously extruded through a syringe-cannulated needle combination, is the most important property for tissue engineering applications. The injectability is always related to the viscosity of materials and may be evaluated based on the force or pressure required to induce a material flow through a needle. The needle length, needle inner diameter, and needle tip shape also affect required force or pressure for injection [49]. Depending on the force required for injection, materials can be rated as very easy to inject (injection force: 0-10 N), easy to inject (11-25 N), injectable (26-100 N), difficult to inject (100-130 N) and very difficult to inject (> 130N) [50]. The measured injection force changes as a function of the aforementioned parameters as derived from the Hagen-Poiseuille equation [51]:

$$f = \frac{32\mu L Q D_s^2}{d^4}$$

where μ is the viscosity (1 s^{-1}), L is the needle length (12.7 mm), Q is the volumetric flow rate (0.3362 mm^3/s), d is the nozzle inner diameter (0.41 mm), and D_s is the inner diameter of the syringe barrel (12.00 mm). The injection force is calculated as 17.4 N, so the gelatin microgel-based composite ink is considered easy to inject for typical applications. While not investigated, the effect of material properties on the injectability can be easily appreciated using the Hagen-Poiseuille equation.

The designed injectable hydrogel-based composite ink benefits from its shear-thinning and self-supporting properties, enabling the printing of complex structures directly in air. For wide printing applications, its printability needs to be characterized, which is one of the most important properties for printing of composite ink-based 3D structures. The printability has been typically evaluated based on the dimensions of deposited filaments [26,52,53]. As such, filaments were printed on microscope glass slides for printability investigation, in particular, in terms of filament width after printing. For the given gelatin-gelatin composite ink printed at a 1.0 mm/s printing path speed, the effect of operating conditions on the printability is assessed based on the nozzle diameter (in terms of nozzle type), standoff distance, material flow rate (in terms of flow rate multiplier), and printing temperature and shown in **Figure 5**.

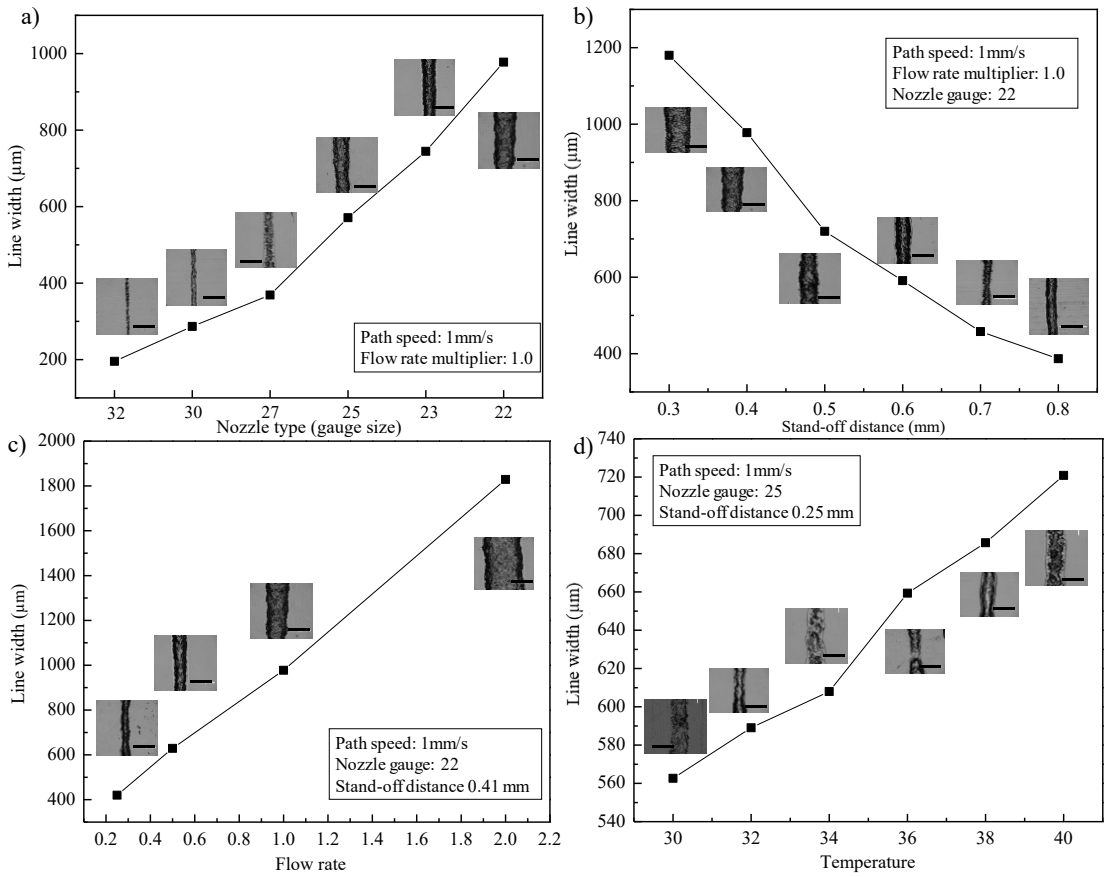

Figure 5. Relationship between operating conditions and filament width. Filament width as a function of (a) nozzle diameter, (b) standoff distance, (c) material flow rate (in terms of an extrusion printers-specific flow rate multiplier), and (d) printing temperature. (Scale bars: 1000 μm).

The geometry of a dispensing tip or nozzle is the basic component for extrusion-based 3D printing, so the effect of the nozzle type on the filament width was firstly investigated: the standoff distance as the nozzle diameter, material flow rate multiplier as 1.0, and printing temperature at 32 °C. **Figure 5a** shows that the filament width can be adjusted accordingly by changing the nozzle type

(in terms of the inner diameter: 100 μm for Gauge 32 nozzles, 150 μm for Gauge 30 nozzles, 200 μm for Gauge 27 nozzles, 250 μm for Gauge 25 nozzles, 330 μm for Gauge 23 nozzles, and 410 μm for Gauge 22 nozzles). As expected, the larger the nozzle diameter, the wider the filament width. The filament is relatively smooth and has no obvious irregular edge due to the sol-gel transition of the composite ink during printing.

Standoff distance is the distance between a dispensing tip and a receiving substrate or a previously printed layer. The effect of standoff distance was investigated based on the following conditions: nozzle gauge of 22, material flow rate as 1.0, and printing temperature at 32 °C. As illustrated in **Figure 5b**, the filament diameter decreases almost linearly with the standoff distance. If the standoff distance is smaller than the height of a printed filament, the nozzle tip may interfere with the deposited filament and make the filament significantly wider. When the standoff distance exceeds a critical value, the filament being dispensed may break up into droplets due to the gravity and dragging force.

The effect of flow rate was studied by modifying a machine-specific flow rate multiplier under the following conditions: nozzle gauge of 22, standoff distance as 0.41 mm, and printing temperature at 32 °C. Since the extrusion printer used in this experiment was ball screw based, the material flow rate is automatically determined based on some pre-set parameters: nozzle type, layer thickness (standoff distance), printing path speed, pulse per nanoliter, and material flow rate multiplier. The flow rate multiplier can be adjusted to fine-tune printing performance and to account for over or under sized filaments based on material properties of inks. The filament width increases linearly with the increasing material flow rate multiplier as shown in **Figure 5c**.

Since gelatin is a thermo-sensitive hydrogel, the influence of temperature on the filament morphology was also examed to determine the optimal printing temperature as follows: nozzle gauge of 25 (a smaller nozzle for printed filaments to be fully imaged), standoff distance as 0.25 mm, and flow rate multiplier as 1.0. An almost linear relationship between the temperature and filament width can be found as seen from **Figure 5d**.

4. Printing Applications of Gelatin Microgel-based Composite Ink

The injectable gelatin microgel-based composite ink is further explored for 3D printing applications based on the printing conditions as identified by following the protocol as shown in **Figure 1b-1**. In particular, tubular structures are printed using the 5% or 10% gelatin microgel-based composite ink for comparison, while all other structures (lattice, cup, overhang, and human anatomical structures) are printed to illustrate the printing capabilities enabled by the designed 10% gelatin microgels (if not specified)-based composite ink. **Figure S4** of **Supporting Information SI4** shows a comparison of dimensions between the designed 3D models and printed 3D structures (tube, cup, overhang structures and human organ structures), which illustrates the printing fidelity when using the designed gelatin microgel-based composite ink.

4.1 Lattice printing

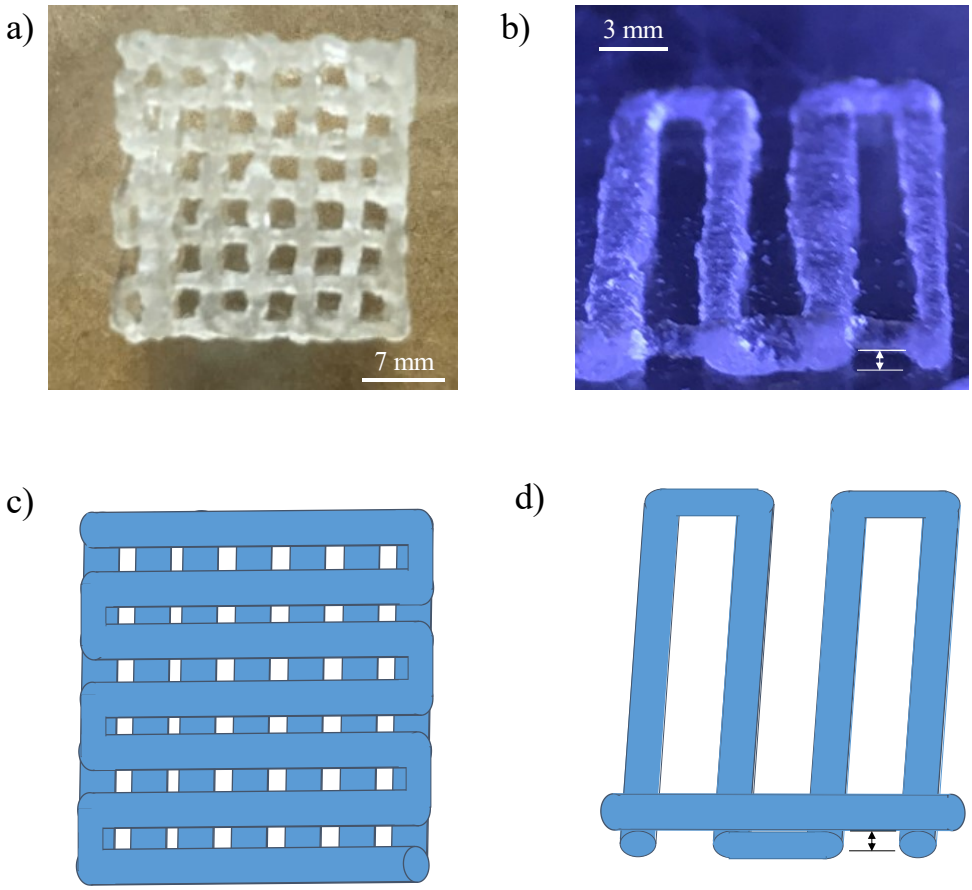

Figure 6. Lattice structures. (a) Top view of a complete structure and (b) isotropic view of first two layers as printed. (c) Isotropic view of a complete structure and (d) side view of first two layers as designed.

Since the gelatin microgel-based composite ink can be used to provide a synthetic substitute ECM as a good scaffold material, herein a multi-layered lattice structure was printed to demonstrate the feasibility of lattice structure printing using the gelatin composite ink. **Figure 6a** and **6b** shows a complete lattice structure and the first two layers of the lattice structure, respectively, and **Figure 6c** and **6d** depicts the corresponding designs. The 21 × 21 mm lattice structure has 8 layers with a total height of 5.6 mm (only part of the lattice is shown due to the imaging limitation), and each

layer consists of a set of 7 parallel filaments, which are perpendicular to those of the adjacent layers. Horizontal gaps (approximately 2.0 mm each) between adjacent filaments are clearly visible in the *xy* plane as illustrated in **Figure 6a** and **6c**. In the Z direction, the vertical gaps between filaments in adjacent layers are approximately 0.4 mm as seen from **Figure 6b**. (The horizontal and vertical gaps can be controlled based on the printing conditions, and such lattice structures with controllable gap or pore sizes can enhance nutrient transport and waste removal.

4.2 Tube and cup printing

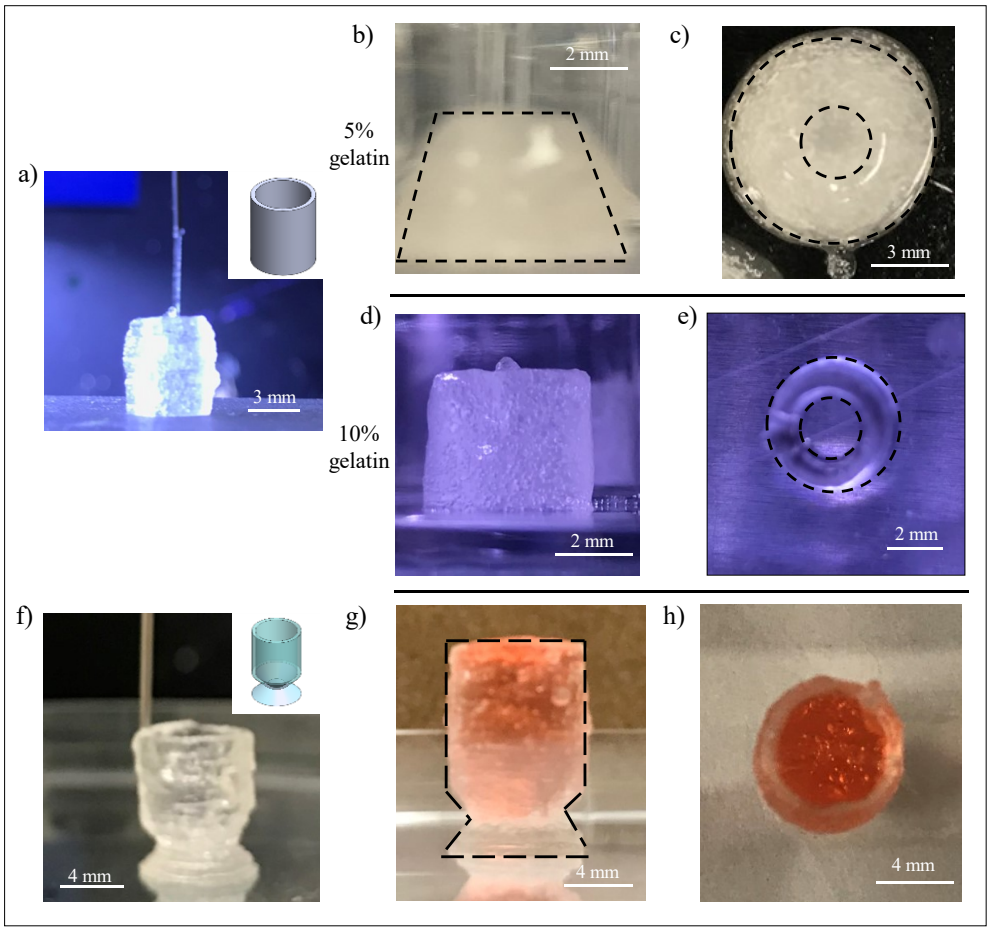

Figure 7. (a) Tube-shaped structure during printing (inset: schematic of tube design). The side view and top view of two printed tube-shaped structures using 5% gelatin microgels (b, c) and 10% gelatin microgels (d, e), respectively. (f) The cup-shaped structure during printing (inset: schematic of cup design). The front view (g) and top view (h) of a printed cup-shaped structure with a dyed water.

Complex 3D structures were printed to show wide printing applications of the gelatin composite ink. Tube printing (**Figure 7a**) shows that the composite ink is printable in air as complex 3D shapes. The tube has a designed height of 6 mm, outer diameter of 5 mm, and wall thickness of 0.4 mm. For comparison, 5% gelatin microgels was also used to print cup-shaped structures. Unfortunately, the tubes printed using the 5% gelatin microgels cannot hold the structure well due to the poor mechanical property as shown in **Figure 7b** and **7c**. In contrast, the surface of the tubes printed using the 10% gelatin microgels is smooth, and the structure holds very well as shown in **Figure 7d** and **7e**.

Furthermore, a cup-shaped structure (**Figure 7f**) was printed to show the feasibility to form 3D enclosed objects from the gelatin microgel-based composite. The cup-shaped construct has a 12 mm height and 8 mm outer diameter, and its overhang inclination angle is 45°. It is noted that some nozzle-induced transient structural deformation is observed during the printing of upper layers; fortunately, the composite ink is elastic enough to revert to the designed shape once the nozzle travels away. The printed cup has high print fidelity as shown in **Figure 7f**, and no leaking is observed after the cup is filled with deionized water containing a red dye for visualization

(**Figure 7g** and **7h**, **Movie M2**), meaning that all deposited layers are connected together flawlessly.

4.3 Overhang structure printing

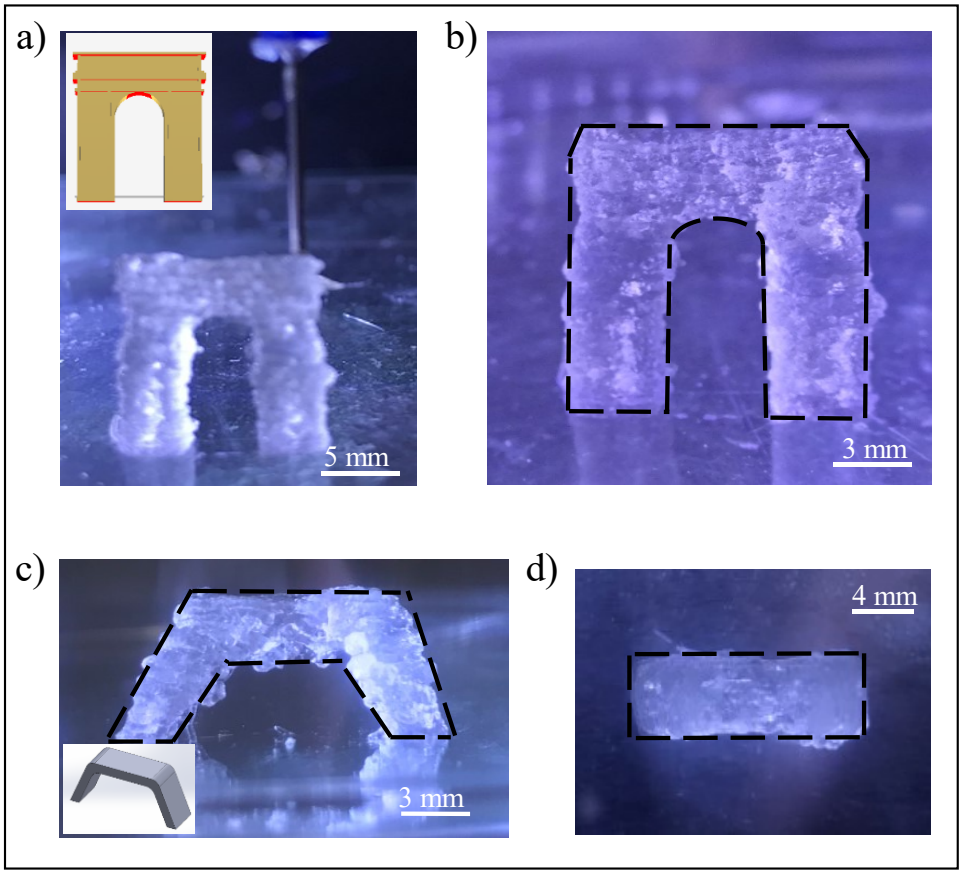

Figure 8. (a) A designed Triumphal Arch during printing (inset: schematic of the designed Triumphal Arch). (b) Front view of a printed triumphal arch. (c) Side view and (d) top view of a printed bridge structure (inset: schematic of the designed bridge structure.)

To further show the self-supporting capability of the gelatin microgel-based composite ink, some overhang structures were printed. **Figure 8a** inset shows a simplified Triumphal Arch with a height of 14 mm and spanning length (width of the gap in the middle) of 10 mm, which is being printed (**Figure 8a**), and **Figure 8b** shows a printed Triumphal Arch. The post of the arch is vertical and has no inclination angle. **Figure 8c** inset shows a designed bridge structure with a width of 4 mm, height of 7.5 mm, and spanning length of 10 mm. The inclination angle of the bridge support is 67°. The shape of the printed bridge is well defined after being printed in air as seen from **Figure 8c** and **8d**. The overhang between two arch posts during printing (**Figure 8a**) and after printing (**Figure 8b**) and the bridge floor (**Figure 8c**) are all flat and have minimal deflection, demonstrating the self-supporting capability of the gelatin microgel-based composite ink.

4.4 Human anatomical structure printing

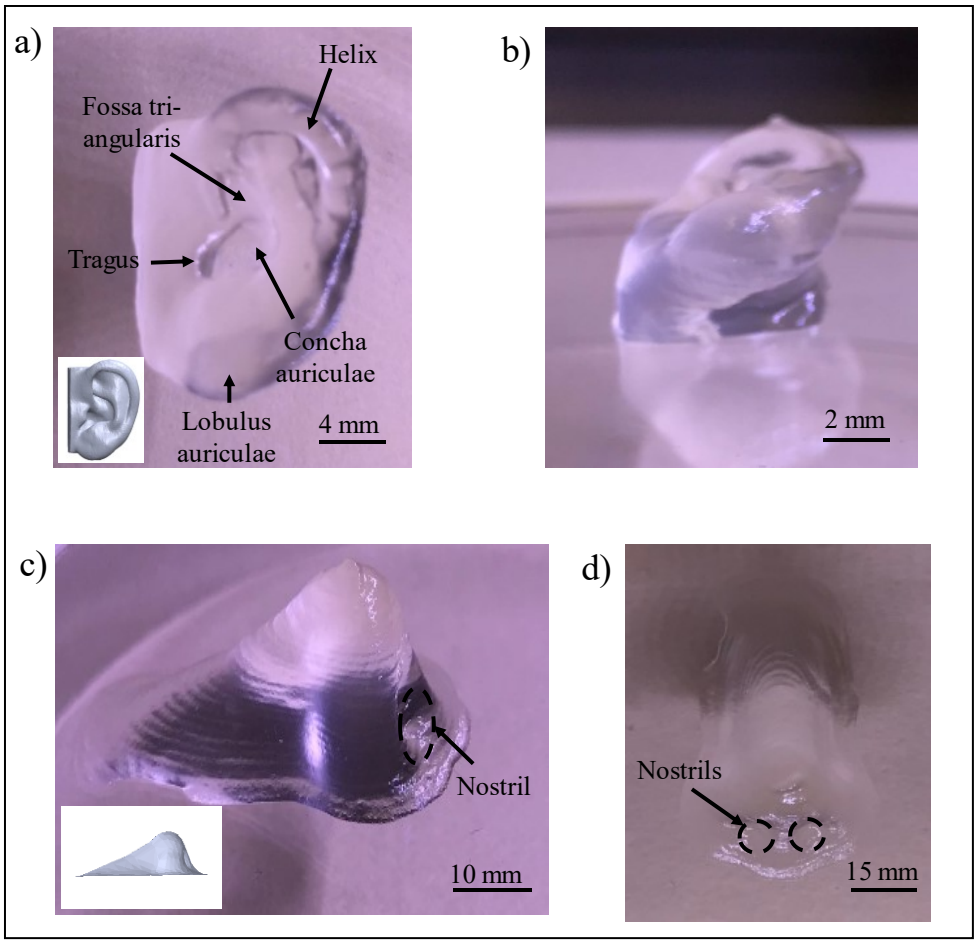

Figure 9. (a) Top view (inset: human ear design) and (b) front view of a printed human ear structure. (c) The front view (inset: human nose design) and (d) top view (d) of a printed human nose structure.

For the demonstration of the potential of the gelatin microgel-based composite ink for complex organ engineering applications, some human anatomical structures were printed (**Movie M3, M4**). **Figure 9a** and its inset illustrates a human ear structure and its design, and the height of the ear is 7.8 mm, and the length is 22 mm. **Figure 9b** and its inset illustrates a human nose structure and its schematic, and it has a height of 30 mm and length of 51.6 mm. The surface of the printed human

ear and nose is very smooth as shown in **Figure 9a-9d**. Some structural characteristics such as helix, fossa tri-angularis, tragus and concha auriculae of the ear and nostrils of the nose are clearly visible, which confirms the potential of the gelatin composite ink for organ printing applications.

5. Assessment of Gelatin Microgel-based Composite Ink for Biomedical Applications

The designed injectable gelatin composite ink is envisioned for 3D bioprinting use such as direct implantation surgeries with a minimally invasive injection procedure and irregular defect/wound filling, to name a few. For it to be applicable in such clinical applications, the designed composite ink should be assessed in terms of its water content, volume shrinkage, and morphology and metabolic activity of encapsulated cells.

5.1 Water content and volume shrinkage assessment

Hydrogels contain numerous hydrophilic polymer networks, which can absorb water up to hundreds of times their dry weight at an equilibrium swelling level. The degree of water content in a hydrogel is an important index to determine the transportation efficiency of nutrients into and waste out of the hydrogel. High water content composite ink formulations have advantages for tissue regeneration because of their better permeability for oxygen, nutrient, and other water-soluble metabolites. The water content of each gelatin composite ink with different microgel gelatin concentrations is shown in **Figure S5a** of **Supporting Information SI5**, it is found that more concentrated gelatin microgels result in a lower water content (11.66 g/g for 5% gelatin microgels, 6.96 g/g for 10% gelatin microgels, and 6.23 g/g for 15% gelatin microgels). All of the designed gelatin microgel-based composite inks have a higher water content than other reported injectable composite hydrogels such as poly(N-isopropylacrylamide) carboxylic acid (PNIPAM-

COOH) (1.25 g/g for 10%) [54], poly(ethylene glycol-b-(dl-lactic acid-co-glycolic acid)-b-ethylene glycol) (PEG–PLGA–PEG) (1.5g/g) [55] and poly(N-isopropylacrylamide-co-2-hydroxyethyl methacrylate-co-methacrylate-polylactide) (Poly(NIPAAm-co-HEMA-co-MAPLA)) (0.87 g/g) [56], which is desirable for tissue engineering and regenerative medicine applications.

Volume stability of injectable hydrogels after injection, printing or implantation is of great importance. The structural stability of the designed gelatin composite ink is evaluated through the volume shrinkage, and the volume shrinkage of various composite hydrogels after gel formation is also compared. As shown in **Figure S5b**, more concentrated gelatin microgels have a lower degree of volume shrinkage, -92.67% for 5% gelatin microgels, -88.99% for 10% gelatin microgels, and -86.05% for 15% gelatin microgels while a typical volume shrinkage ratio is -85.5% to -98.3% [57,58]. From a tissue engineering, volumetric contraction in scaffolds may have several deleterious effects such as damaging encapsulated cells and squeezing encapsulated cells out of the scaffold. Therefore, the addition of gelatin microgels help improve the volume stability and provide a better, long-lasting physiological environment.

5.2 Biocompatibility evaluation

The biocompatibility of the gelatin microgel-based composite was evaluated based on the morphology and metabolic activity of NIH 3T3 mouse fibroblasts encapsulated in the gelatin microgel-based composite ink. Specifically, straight cellular tubes with a wall thickness of 0.4 mm were directly printed in the air. **Figure 10a** and **10b** shows that the cells survive well (dyed in green) in the printed structures after printing as well as 14 days of static incubation.

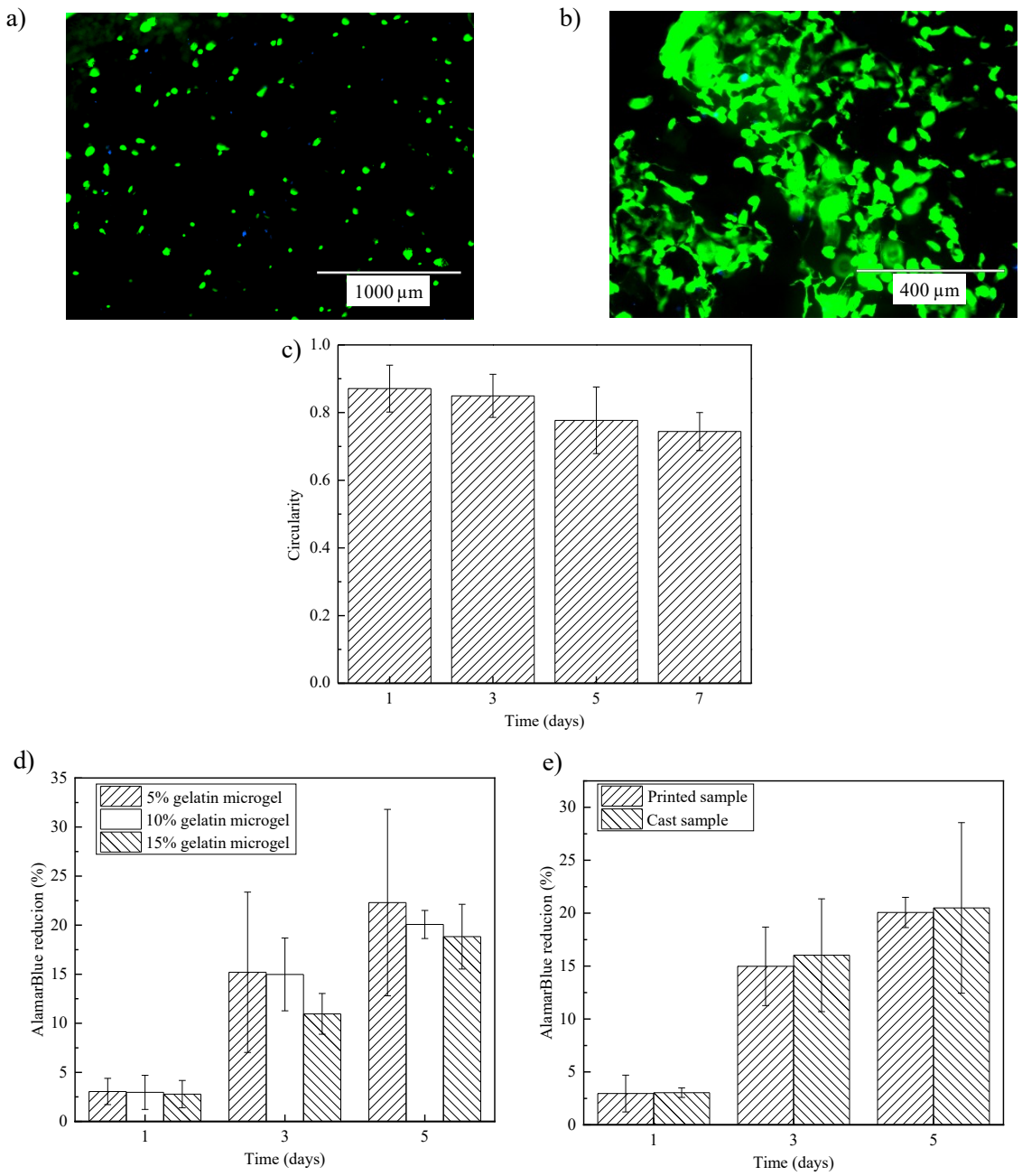

Figure 10. Biocompatibility evaluations of the designed gelatin composite ink. Cell morphology (a) right after printing and (b) after culturing for 14 days. (c) The cell circularity as a function of culture time. (d) AlamarBlue reduction percentage differences with different gelatin concentration for microgels. (e) AlamarBlue reduction percentage differences between printed sample and cast sample.

For better quantitatively assessing the morphology difference of cells, the circularity of the living cells cultured for 1, 3, 5 and 7 days were calculated respectively. The circularity ($4\pi \times$ area/perimeter^2), ranging from 0 to 1, describes the roundness of a cell, and 1 indicates cells with a perfectly circular shape. Generally, the calculated circularity of encapsulated cells is bimodal, with two distinct sub-populations: 1) rounded with high circularity, which indicates low cell spreading, and 2) elongated with low circularity, which indicates extensive spreading. Average circularity data for cells cultured after different durations are presented in **Figure 10c**. The circularity of the living cells decreases over time meaning that the cells are spreading and showing good cell-scaffold interactions analogous to those found in native ECMs.

In addition, AlamarBlue reduction testing was conducted on the printed and cast cell-laden gelatin microgel-based composite specimens with different microgel gelatin concentrations to assess the cell metabolic activity after 1, 3, and 5 days. The AlamarBlue reduction index of different microgel gelatin concentrations was investigated and is shown in **Figure 10d**. The lower concentration gelatin microgels support higher metabolic activity (in terms of higher metabolic reduction percentages) for the cells since there are relatively few polymer chains to inhibit diffusion, which supplies nutrients and removes waste from the cells throughout the bulk construct. As seen from **Figure 10e**, the cells within the samples and cast samples have similar metabolic activity, and the AlamarBlue reduction index increases over time, indicating the feasibility of using the gelatin microgel-based composite ink for the direct printing in air approach for its cytocompatibility and ability in supporting of cell proliferation.

6. Conclusions and Future Work

Microgel-based 3D bioprinting ink design is a valuable tool for improving the printability of desirable build materials without including non-ideal components in the overall formulation. This concept is demonstrated herein using gelatin as a model biomaterial, which has intrinsic non-ideal printing behavior. By pre-processing the gelatin into covalently cross-linked microgels, a fully biocompatible rheology modifier is obtained. In combination with a curable gelatin solution phase, the two-phase gelatin microgel-based composite ink is injectable, solidifies quickly after injection, and enables convenient fabrication of constructs from only gelatin, without the need for any other polymeric or inorganic materials to facilitate the fabrication process as demonstrated during the printing of lattice, tube-shaped, cup-shaped, and human anatomical structures in air. In addition to reducing the ink formulation complexity, this composite ink approach may facilitate translation of 3D bioprinted constructs to clinical applications because gelatin has been approved by regulatory agencies for clinical use in other devices.

Future work may include further investigation of the preparation of smaller and monodieperse gelatin microgels, the effect of the microgel component on the printing process in terms of rheology, shape fidelity, and cell viability, evaluation of other biopolymers for the discrete microgel and continuous solution phases, application of this ink design to print more complex and physiologically relevant structures with different cells (e.g. chondrocytes, urine-derived stem cells, induced pluripotent stem cells, etc.) for tissue regeneration for *in vivo* and *in vitro* tests and direct injection/printing over soft and hard tissues *in vivo*, systematic testing of the time -dependent stability of printed structures and more extensive post-printing evaluations of functionality such as the effect of 3D gelatin environment on cell performance.

7. Experimental Section

7.1 Preparation of gelatin-based microgel composite ink

For the preparation of 10.0% gelatin-based microgels, 10.5% w/v gelatin (225 bloom type A, MP Biomedicals, Solon, OH) powder was dissolved in phosphate buffered saline (PBS, Corning cellgro, Manassas, VA) at 37°C in a silver bead bath for 30 minutes. The 20.0% w/v transglutaminase (TG) (Moo Gloo TI Transglutaminase Formula, Modernist Pantry, York, ME) stock solution was prepared by dissolving TG powder in PBS, vortex mixing gently, and then incubating in a 37°C bead bath for 30 minutes. These two solutions were mixed at a 19:1 ratio for a final concentration of 10.0% w/v gelatin and 1.0% TG. Then the mixed solution was incubated in a 37°C silver bead bath for 4 hours for gelatin cross-linking. For comparison, 5.0% and 15.0% w/v gelatin gels were prepared similarly, keeping the gelatin to TG ratio of 10:1 (that is, the TG concentration was 0.5% and 1.5% w/v, respectively). The cross-linked gelatin gel was heated in a 100°C water bath for 30 minutes to deactivate TG. Furthermore, the cross-linked gel was blended using a household blender (3-speed hand blender, KitchenAid, Benton Harbor, MI) at the highest speed for 5 minutes with 200 mL deionized (DI) water added in the blending jar. After blending, the microgel mixture was centrifuged at 4200 rpm for 5 minutes to remove extra water. Then, the packed microgels were mixed with an equal volume of PBS and autoclaved at 121°C for 60 min. The sterilized microgels were recollected by centrifuging at 4200 rpm for 5 minutes and stored at 4°C until use; after sterilization, the microgels were handled in a biosafety cabinet using an aseptic technique.

For the preparation of gelatin microgel-based composite ink, the gelatin microgels were mixed with gelatin dry powders at 3% w/v. The mixture was mixed thoroughly with a glass rod and then

incubated in a 37°C bead bath for 30 minutes until the gelatin powder was completely dissolved. The composite ink was loaded in the printer cartridge assembled with the heated printhead for structure printing. For mechanical testing, TG stock was added to the composite ink to reach a final concentration of 0.5% w/v TG immediately before casting the dog bone test specimens.

7.2 Printing protocols

All printing was carried out using a ball screw motion controlled extrusion microdispensing machine (Hyrel Engine SR, Hyrel3D, Norcross, GA) with a warm flow head (KRA-15, Hyrel3D, Norcross, GA). The prepared cell ink was extruded from a 22 gauge nozzle (0.41 mm inner diameter, EFD Nordson, Vilters, Switzerland) with a nozzle temperature of 32°C to achieve optimal printing performance. The layer height was set to 0.41 mm and flow rate multiplier was 1.0. All structures were printed using a tip travel speed of 1 mm/sec. For large scale structures that need more than 45 minutes to print, after printing, structures were placed in the refrigerator at 4°C for at least 30 minutes for thermal gelation. Then chilled constructs were treated with TG in PBS at 30°C for covalent cross-linking to form physiologically stable constructs. For small scale structures, which can be finished in 45 minutes, after printing, structures were put into 37°C bead bath for 30 minutes for covalent cross-linking to form physiologically stable constructs since TG was pre-mixed with the composite ink.

For the printability study, all of the printing path codes were programmed manually as custom G-code scripts. For the complex 3D structure printing, all of the 3D structure models were designed through SolidWorks (Dassault Systemes SolidWorks Corp, Waltham, MA) and exported as STL files except the 3D models of nose and ear structures, which were downloaded from Thingiverse

(http://www.thingiverse.com/) directly as STL files. The STL files were prepared using the Slic3r tools embedded in the Repetrel control software of the Hyrel 3D printer. The G-code was generated automatically after slicing.

7.3 Rheological property measurement

Rheological properties of the gelatin microgel-based composite ink with 5% gelatin microgels, 10% gelatin microgels and 15% gelatin microgels were measured as in a previous study [61]. Strain sweeps (strain range: 1% to 100%) were performed at a low frequency (1 Hz) for the gelatin microgel-based composite ink formulations to determine the linear viscoelasticity region (LVR) and the yield-stress value. Samples were pre-sheared at 100 s^{-1} for 30 seconds followed by a waiting period for a 60 seconds recovery period to eliminate loading effects. Steady rate sweeps were conducted at a low strain (1%) to confirm the shear-thinning property of the composite ink for a shear rate range from 0.01 s^{-1} to 100 s^{-1}. To explore the transition between solid-like and fluid-like behavior, all gelatin microgel-based composite inks were characterized using cyclic oscillatory shear between 1% and 100% strain at low frequency (1 Hz) for 300 seconds at each strain amplitude. For the sol-gel transition behavior investigation, only 3% gelatin solution was characterized using a temperature sweep at a scanning rate of 0.01 ºC/sec at a low frequency (1 Hz) and low strain (1%). For the response time of viscosity after shearing, the gelatin microgel-based composite ink was pre-sheared at a shear rate of 100 s^{-1} for 10 seconds after which the shear rate was reduced to 0 s^{-1} and the viscosity change was recorded during the following 10 seconds.

7.4 Mechanical property measurement.

Mechanical properties of cross-linked gelatin microgel-based composites were measured separately using a micro tester (eXpert 4000, admet, Norwood, NA). The composite ink formulations with 5% gelatin microgels, 10% gelatin microgels, and 15% gelatin microgels were cast in dog bone shaped molds as shown in **Supporting Information SI3** with a cross section of 1.60 mm× 2.00 mm, and an equivalent structure was printed using the composite ink formulation with 10% gelatin microgels for comparison. All of the tensile tests were performed at a jog rate of 1 mm/sec. The load data was collected using the 1000 g load sensor and the motion stopped at the 90% of the maximum load. The stress-strain curve was generated according to the load, displacement and sample shape. The Young's modulus of the gelatin microgel-based composites were calculated through the linear region of the stress-strain curve.

7.5 Gelatin particle size measurement.

Particle size of gelatin microgels was measured using a particle characterization machine (LS320, Beckman Coulter, Brea, CA) based on laser light scattering. 10% gelatin gel blended for 3 minutes, 5 minutes and 7 minutes was characterized to illustrate the effect of the blending time. 5% gelatin, 10% gelatin and 15% gelatin gel blended for 5 minutes were characterized to determine the relationship between microgel particle size and gelatin concentration. Each sample type was measured in triplicate with a measurement time of 60 seconds.

7.6 Water content and volume shrinkage study

To examine the water content of the designed composite inks, the cross-linked 5% gelatin, 10% gelatin, and 15% gelatin composites were immersed into phosphate buffered saline (PBS) for 1 hour at 37°C to ensure complete hydration. Then the composites were removed from PBS,

weighed, placed in Petri dishes, dried at 37°C for 24 hours, and finally weighed to determine the dry weight of each of the composites. The water content of the designed composites was determined from the weight differences of composites before and after drying:

$$Water\ content = \frac{W_{wet} - W_{dry}}{W_{dry}}$$

where W_{wet} is the weight of the designed composites after gelation and immersion at 37 °C, and W_{dry} is the dry weight of the composites. The mass of residual salt from PBS is negligible compared to the mass of the polymer.

The volume shrinkage (%) of the designed composite ink was defined as the water volume loss percentage after drying for 24 hours.

$$Volume\ shrinkage\,(\%) = -(1 - \frac{V_i - V_{H20}}{V_i}) \times 100\% = -\frac{V_{H20}}{V_i} \times 100\%$$

where V_i is the volume of initial composite ink and V_{H20} is the volume of the water loss.

7.7 Cellular structure studies

Cellular ink was prepared by suspending NIH 3T3 mouse fibroblasts (ATCC, Rockville, MD) in the warm gelatin microgel-based composite ink with a final concentration of 1×10^5 cells/mL. The re-suspended 3T3 mouse fibroblasts cells with a cell concentration of 1×10^7 cells/mL were prepared as described in a previous study [59]. The re-suspended cells were added to the warmed ink mixture to produce inks with final concentrations of 3% gelatin and 1×10^5 cells/mL in packed 5% (w/v), 10% (w/v) and 15% (w/v) gelatin microgels respectively. TG stock was added to the composite ink to reach the final concentration of 0.5% w/v TG immediately before cellular

structure printing. The cellular ink was loaded in a sterilized KRA-15 cartridge for printing. Printing parameters for cellular structures are specified in Section 2.2.

The printed 10% gelatin microgel-based composite with 3T3 cellular structures were placed in a 24-well plate and incubated for 30 minutes at 37°C in a humidified 5.0% CO_2 incubator for gelatin-TG cross-linking. After cross-linking the printed cellular structures were cultured as described in a previous study [51].

The cell morphology within the constructs was evaluated on day 0 and day 14 using fluorescent staining as described in a previous study [61], where the green color represents live cells and the blue color represents cell nuclei. For metabolic activity quantification in the printed cellular structures and cast cellular structures, 100 μL of 5%, 10% and 15% cellular ink with 1×10^5 cells/mL, respectively, were printed or cast in a 96-well plate. After incubation for 45 minutes in a 37°C bead bath for cross-linking, the specimens were cultured as described in a previous study [51]. The cytocompatibility of the cellular structures was evaluated by the AlamarBlue assay on Days 1, 3 and 5 as described in a previous study [60]. Briefly, on each testing day, the cell medium was removed, and then 80 μL cell medium with 10% (v/v) AlamarBlue was added in each well and incubated for 2 hours. The reducing activity, which correlates to the population of living cells, was quantitatively measured with a fluorescence microplate reader (Synergy HT, Biotek, Winooski, VT). The circularity of the living cells in the printed and cast constructs was measured based on the cell morphology on Day 1, 3, 5 and 7 by outlining isolated cells with ImageJ (NIH, Bethesda, Maryland) for more than 50 cells per condition.

7.8 Statistical analysis

All quantitative values of this article in the text and figures were assessed as means ± standard deviation (SD) in triplicate for each sample type. Analysis of variance (ANOVA) was conducted herein for statistical analysis, and $p < 0.05$ was considered statistically significant.

List of Supporting Information

Supporting Information SI1: Rheological property measurement of gelatin composite ink. (PDF)

Supporting Information SI2: Effect of temperature on composite ink extrusion. (PDF)

Supporting Information SI3: Mechanical property measurement of gelatin composite parts. (PDF)

Supporting Information SI4: Analysis of the dimension fidelity of printed structures. (PDF)

Supporting Information SI5: Analysis of water content and volume shrinkage of gelatin composites. (PDF)

Supporting Information M1: Movie of dog bone-shaped specimen under tensile testing. (Movie)

Supporting Information M2: Movie of cup-shaped structure printing in air. (Movie)

Supporting Information M3: Movie of human ear-shaped structure printing in air. (Movie)

Supporting Information M4: Movie of human nose-shaped structure printing in air. (Movie)

Acknowledgements

This study was partially supported by the US National Science Foundation (1762941), and the use of Anton Paar rheometer is acknowledged.

Competing financial interests

This work has been disclosed to the Office of Technology Licensing at the University of Florida.

REFERENCES:

1. Langer, R.; Vacanti, J. Tissue Engineering. *Science* 1993, *260* (5110), 920–926.
2. Drury, J. L.; Mooney, D. J. Hydrogels for Tissue Engineering: Scaffold Design Variables and Applications. *Biomaterials* 2003, *24* (24), 4337–4351.
3. Slaughter, B. V.; Khurshid, S. S.; Fisher, O. Z.; Khademhosseini, A.; Peppas, N. A. Hydrogels in Regenerative Medicine. *Advanced Materials* 2009, *21* (32-33), 3307–3329.
4. Vlierberghe, S. V.; Dubruel, P.; Schacht, E. Biopolymer-Based Hydrogels As Scaffolds for Tissue Engineering Applications: A Review. *Biomacromolecules* 2011, *12* (5), 1387–1408.
5. Choi, B.; Kim, S.; Lin, B.; Wu, B. M.; Lee, M. Cartilaginous Extracellular Matrix-Modified Chitosan Hydrogels for Cartilage Tissue Engineering. *ACS Applied Materials & Interfaces* 2014, *6* (22), 20110–20121.
6. Yazdimamaghani, M.; Vashaee, D.; Assefa, S.; Walker, K. .j.; Madihally, S. V.; Köhler, G. .a.; Tayebi, L. Hybrid Macroporous Gelatin/Bioactive-Glass/Nanosilver Scaffolds with Controlled Degradation Behavior and Antimicrobial Activity for Bone Tissue Engineering. *Journal of Biomedical Nanotechnology* 2014, *10* (6), 911–931.
7. Wei, Y.; Hu, Y.; Hao, W.; Han, Y.; Meng, G.; Zhang, D.; Wu, Z.; Wang, H. A Novel Injectable Scaffold for Cartilage Tissue Engineering Using Adipose-Derived Adult Stem Cells. *Journal of Orthopaedic Research* 2008, *26* (1), 27–33.
8. Jin, R.; Teixeira, L. M.; Dijkstra, P.; Karperien, M.; Blitterswijk, C. V.; Zhong, Z.; Feijen, J. Injectable Chitosan-Based Hydrogels for Cartilage Tissue Engineering. *Biomaterials* 2009, *30* (13), 2544–2551.

9. Gong, Y.; Wang, C.; Lai, R. C.; Su, K.; Zhang, F.; Wang, D.-A. An Improved Injectable Polysaccharide Hydrogel: Modified Gellan Gum for Long-Term Cartilage Regeneration in Vitro. *Journal of Materials Chemistry* 2009, *19* (14), 1968.

10. Tan, H.; Li, H.; Rubin, J. P.; Marra, K. G. Controlled Gelation and Degradation Rates of Injectable Hyaluronic Acid-Based Hydrogels through a Double Crosslinking Strategy. *Journal of Tissue Engineering and Regenerative Medicine* 2011, *5* (10), 790–797.

11. Sivashanmugam, A.; Kumar, R. A.; Priya, M. V.; Nair, S. V.; Jayakumar, R. An Overview of Injectable Polymeric Hydrogels for Tissue Engineering. *European Polymer Journal* 2015, *72*, 543–565.

12. O'Hara, R.; Buchanan, F.; Dunne, N. Injectable Calcium Phosphate Cements for Spinal Bone Repair. *Biomaterials for Bone Regeneration* 2014, 26–61.

13. Overstreet, D. J.; Dutta, D.; Stabenfeldt, S. E.; Vernon, B. L. Injectable Hydrogels. *Journal of Polymer Science Part B: Polymer Physics* 2012, *50* (13), 881–903.

14. Amini, A. A.; Nair, L. S. Injectable Hydrogels for Bone and Cartilage Repair. *Biomedical Materials* 2012, *7* (2), 024105.

15. Binetti, V. R.; Fussell, G. W.; Lowman, A. M. Evaluation of Two Chemical Crosslinking Methods of Poly(Vinyl Alcohol) Hydrogels for Injectable Nucleus Pulposus Replacement. *Journal of Applied Polymer Science* 2014, *131* (19).

16. Shen, Z.-S.; Cui, X.; Hou, R.-X.; Li, Q.; Deng, H.-X.; Fu, J. Tough Biodegradable Chitosan–Gelatin Hydrogels via in Situ Precipitation for Potential Cartilage Tissue Engineering. *RSC Advances* 2015, *5* (69), 55640–55647.

17. Hong, Y.; Gong, Y.; Gao, C.; Shen, J. Collagen-Coated Polylactide Microcarriers/Chitosan Hydrogel Composite: Injectable Scaffold for Cartilage Regeneration. *Journal of Biomedical Materials Research Part A* 2008, *85A* (3), 628–637.

18. Bidarra, S. J.; Barrias, C. C.; Granja, P. L. Injectable Alginate Hydrogels for Cell Delivery in Tissue Engineering. *Acta Biomaterialia* 2014, *10* (4), 1646–1662.

19. Dorsey, S. M.; Mcgarvey, J. R.; Wang, H.; Nikou, A.; Arama, L.; Koomalsingh, K. J.; Kondo, N.; Gorman, J. H.; Pilla, J. J.; Gorman, R. C.; Wenk, J. F.; Burdick, J. A. MRI Evaluation of Injectable Hyaluronic Acid-Based Hydrogel Therapy to Limit Ventricular Remodeling after Myocardial Infarction. *Biomaterials* 2015, *69*, 65–75.

20. Sim, H. J.; Thambi, T.; Lee, D. S. Heparin-Based Temperature-Sensitive Injectable Hydrogels for Protein Delivery. *Journal of Materials Chemistry B* 2015, *3* (45), 8892–8901.

21. Wang, F.; Li, Z.; Khan, M.; Tamama, K.; Kuppusamy, P.; Wagner, W. R.; Sen, C. K.; Guan, J. Injectable, Rapid Gelling and Highly Flexible Hydrogel Composites as Growth Factor and Cell Carriers. *Acta Biomaterialia* 2010, *6* (6), 1978–1991.

22. Alexander, A.; Ajazuddin; Khan, J.; Saraf, S.; Saraf, S. Poly(Ethylene Glycol)–Poly(Lactic-Co-Glycolic Acid) Based Thermosensitive Injectable Hydrogels for Biomedical Applications. *Journal of Controlled Release* 2013, *172* (3), 715–729.

23. Jian, H.; Wang, M.; Dong, Q.; Li, J.; Wang, A.; Li, X.; Ren, P.; Bai, S. Dipeptide Self-Assembled Hydrogels with Tunable Mechanical Properties and Degradability for 3D Bioprinting. ACS Applied Materials & Interfaces 2019, 11 (50), 46419–46426.

24. Ossipov, D. A.; Piskounova, S.; Hilborn Jöns. Poly(Vinyl Alcohol) Cross-Linkers for in Vivo Injectable Hydrogels. *Macromolecules* 2008, *41* (11), 3971–3982.

25. Huang, Y.; Schmid, S. R. Additive Manufacturing for Health: State of the Art, Gaps and Needs, and Recommendations. *Journal of Manufacturing Science and Engineering* 2018, *140* (9), 094001.

26. Zhang, Z.; Jin, Y.; Yin, J.; Xu, C.; Xiong, R.; Christensen, K.; Ringeisen, B. R.; Chrisey, D. B.; Huang, Y. Evaluation of Bioink Printability for Bioprinting Applications. *Applied Physics Reviews* 2018, *5* (4), 041304.

27. Kaklamani, G.; Cheneler, D.; Grover, L. M.; Adams, M. J.; Bowen, J. Mechanical Properties of Alginate Hydrogels Manufactured Using External Gelation. *Journal of the Mechanical Behavior of Biomedical Materials* 2014, *36*, 135–142.

28. Milazzo, M.; Negrini, N. C.; Scialla, S.; Marelli, B.; Farè, S.; Danti, S.; Buehler, M. J. Additive Manufacturing Approaches for Hydroxyapatite-Reinforced Composites. *Advanced Functional Materials* 2019, *29* (35), 1903055.

29. Lee, K. Y.; Mooney, D. J. Hydrogels for Tissue Engineering. *Chemical Reviews* 2001, *101* (7), 1869–1880.

30. Lakouraj, M. M.; Tajbakhsh, T; Mokhtary. M. Synthesis and swelling characterization of cross-linked PVP/PVA hydrogels. *Iranian Polymer Journal* 2005,*14* (12), 1022-1030.

31. Schuurman, W.; Levett, P. A.; Pot, M. W.; Weeren, P. R. V.; Dhert, W. J. A.; Hutmacher, D. W.; Melchels, F. P. W.; Klein, T. J.; Malda, J. Gelatin-Methacrylamide Hydrogels as Potential Biomaterials for Fabrication of Tissue-Engineered Cartilage Constructs. *Macromolecular Bioscience* 2013, *13* (5), 551–561.

32. Su, K.; Wang, C. Recent Advances in the Use of Gelatin in Biomedical Research. *Biotechnology Letters* 2015, *37* (11), 2139–2145.

33. Yue, K.; Santiago, G. T.-D.; Alvarez, M. M.; Tamayol, A.; Annabi, N.; Khademhosseini, A. Synthesis, Properties, and Biomedical Applications of Gelatin Methacryloyl (GelMA) Hydrogels. *Biomaterials* 2015, *73*, 254–271.

34. Klotz, B. J.; Gawlitta, D.; Rosenberg, A. J.; Malda, J.; Melchels, F. P. Gelatin-Methacryloyl Hydrogels: Towards Biofabrication-Based Tissue Repair. *Trends in Biotechnology* 2016, *34* (5), 394–407.

35. Pepelanova, I.; Kruppa, K.; Scheper, T.; Lavrentieva, A. Gelatin-Methacryloyl (GelMA) Hydrogels with Defined Degree of Functionalization as a Versatile Toolkit for 3D Cell Culture and Extrusion Bioprinting. *Bioengineering* 2018, *5* (3), 55.

36. Ketz, R. J.; Prudhomme, R. K.; Graessley, W. W. Rheology of Concentrated Microgel Solutions. *Rheologica Acta* 1988, *27* (5), 531–539.

37. Cates, M. E.; Wittmer, J. P.; Bouchaud, J.-P.; Claudin, P. Jamming, Force Chains, and Fragile Matter. *Physical Review Letters* 1998, *81* (9), 1841–1844.

38. Liu, A. J.; Nagel, S. R. Jamming Is Not Just Cool Any More. *Nature* 1998, *396* (6706), 21–22.

39. O'Hern, C. S.; Silbert, L. E.; Liu, A. J.; Nagel, S. R. Jamming at Zero Temperature and Zero Applied Stress: The Epitome of Disorder. *Physical Review E* 2003, *68* (1), 011306.

40. Menut, P.; Seiffert, S.; Sprakel, J.; Weitz, D. A. Does Size Matter? Elasticity of Compressed Suspensions of Colloidal- and Granular-Scale Microgels. *Soft Matter* 2012, *8* (1), 156–164.

41. Nakamura, M.; Nishiyama, Y.; Henmi, C.; Iwanaga, S.; Nakagawa, H.; Yamaguchi, K.; Akita, K.; Mochizuki, S.; Takiura, K. Ink Jet Three-Dimensional Digital Fabrication for Biological Tissue Manufacturing: Analysis of Alginate Microgel Beads Produced by Ink Jet

Droplets for Three Dimensional Tissue Fabrication. *Journal of Imaging Science and Technology* 2008, *52* (6), 060201.

42. Highley, C. B.; Song, K. H.; Daly, A. C.; Burdick, J. A. Jammed Microgel Inks for 3D Printing Applications. *Advanced Science* 2018, *6* (1), 1801076.

43. Yung, C.; Wu, L.; Tullman, J.; Payne, G.; Bentley, W.; Barbari, T. Transglutaminase Crosslinked Gelatin as a Tissue Engineering Scaffold. *Journal of Biomedical Materials Research Part A* 2007, *83A* (4), 1039–1046.

44. Christensen, K.; Davis, B.; Jin, Y.; Huang, Y. Effects of Printing-Induced Interfaces on Localized Strain within 3D Printed Hydrogel Structures. *Materials Science and Engineering: C* 2018, *89*, 65–74.

45. Compaan, A. M.; Song, K.; Chai, W.; Huang, Y. Cross-Linkable Microgel Composite Matrix Bath for Embedded Bioprinting of Perfusable Tissue Constructs and Sculpting of Solid Objects. *ACS Applied Materials & Interfaces* 2020. 10.1021/acsami.9b15451

46. Shao, L.; Gao, Q.; Zhao, H.; Xie, C.; Fu, J.; Liu, Z.; Xiang, M.; He, Y. Fiber-Based Mini Tissue with Morphology-Controllable GelMA Microfibers. *Small* 2018, *14* (44), 1802187.

47. Shin, H.; Olsen, B. D.; Khademhosseini, A. The Mechanical Properties and Cytotoxicity of Cell-Laden Double-Network Hydrogels Based on Photocrosslinkable Gelatin and Gellan Gum Biomacromolecules. *Biomaterials* 2012, *33* (11), 3143–3152.

48. Hassanzadeh, P.; Kazemzadeh-Narbat, M.; Rosenzweig, R.; Zhang, X.; Khademhosseini, A.; Annabi, N.; Rolandi, M. Ultrastrong and Flexible Hybrid Hydrogels Based on Solution Self-Assembly of Chitin Nanofibers in Gelatin Methacryloyl (GelMA). *Journal of Materials Chemistry B* 2016, *4* (15), 2539–2543.

49. Cilurzo, F.; Selmin, F.; Minghetti, P.; Adami, M.; Bertoni, E.; Lauria, S.; Montanari, L. Injectability Evaluation: An Open Issue. *AAPS PharmSciTech* 2011, *12* (2), 604–609.

50. Rungseevijitprapa, W.; Bodmeier, R. Injectability of Biodegradable in Situ Forming Microparticle Systems (ISM). *European Journal of Pharmaceutical Sciences* 2009, *36* (4-5), 524–531.

51. Watt, R. P.; Khatri, H.; Dibble, A. R. Injectability as a Function of Viscosity and Dosing Materials for Subcutaneous Administration. *International Journal of Pharmaceutics* 2019, *554*, 376–386.

52. Jin, Y.; Chai, W.; Huang, Y. Printability Study of Hydrogel Solution Extrusion in Nanoclay Yield-Stress Bath during Printing-Then-Gelation Biofabrication. *Materials Science and Engineering: C* 2017, *80*, 313–325.

53. Jin, Y.; Liu, C.; Chai, W.; Compaan, A.; Huang, Y. Self-Supporting Nanoclay as Internal Scaffold Material for Direct Printing of Soft Hydrogel Composite Structures in Air. *ACS Applied Materials & Interfaces* 2017, *9* (20), 17456–17465.

54. Chen, J.-P.; Cheng, T.-H. Preparation and Evaluation of Thermo-Reversible Copolymer Hydrogels Containing Chitosan and Hyaluronic Acid as Injectable Cell Carriers. *Polymer* 2009, *50* (1), 107–116.

55. Jeong, B.; Bae, Y. H.; Kim, S. W. Drug Release from Biodegradable Injectable Thermosensitive Hydrogel of PEG–PLGA–PEG Triblock Copolymers. *Journal of Controlled Release* 2000, *63* (1-2), 155–163.

56. Ma, Z.; Nelson, D. M.; Hong, Y.; Wagner, W. R. Thermally Responsive Injectable Hydrogel Incorporating Methacrylate-Polylactide for Hydrolytic Lability. *Biomacromolecules* 2010, *11* (7), 1873–1881.

57. Konishi, M.; Tabata, Y.; Kariya, M.; Hosseinkhani, H.; Suzuki, A.; Fukuhara, K.; Mandai, M.; Takakura, K.; Fujii, S. In Vivo Anti-Tumor Effect of Dual Release of Cisplatin and Adriamycin from Biodegradable Gelatin Hydrogel. *Journal of Controlled Release* 2005, *103* (1), 7–19.

58. Tabata, Y.; Ikada, Y. Vascularization Effect of Basic Fibroblast Growth Factor Released from Gelatin Hydrogels with Different Biodegradabilities. *Biomaterials* 1999, *20* (22), 2169–2175.

59. Zhang, Z.; Xu, C.; Xiong, R.; Chrisey, D. B.; Huang, Y. Effects of Living Cells on the Bioink Printability during Laser Printing. *Biomicrofluidics* 2017, *11* (3), 034120.

60. Jin, Y.; Compaan, A.; Chai, W.; Huang, Y. Functional Nanoclay Suspension for Printing-Then-Solidification of Liquid Materials. *ACS Applied Materials & Interfaces* 2017, *9* (23), 20057–20066.

61. Compaan, A. M.; Song, K.; Huang, Y. Gellan Fluid Gel as a Versatile Support Bath Material for Fluid Extrusion Bioprinting. *ACS Applied Materials & Interfaces* 2019, *11* (6), 5714–5726.

Table of Contents Graph